June 2000 • NREL/CP-520-28569

Conference Paper

# Silicon Float-Zone Crystal Growth as a Tool for the Study of Defects and Impurities

## Preprint

T.F. Ciszek and T.H. Wang

*To be presented at the Electrochemical Society Fall Conference*
*Phoenix, Arizona*
*October 22-27, 2000*

**National Renewable Energy Laboratory**

**1617 Cole Boulevard**
**Golden, Colorado 80401-3393**

**NREL is a U.S. Department of Energy Laboratory**
**Operated by Midwest Research Institute • Battelle • Bechtel**

**Contract No. DE-AC36-99-GO10337**

# SILICON FLOAT-ZONE CRYSTAL GROWTH AS A TOOL FOR THE STUDY OF DEFECTS AND IMPURITIES

T. F. Ciszek and T.H. Wang
National Renewable Energy Laboratory
Golden, Colorado 80401 U.S.A.

## ABSTRACT

Because of its ability to produce silicon crystals of exceptionally high purity and crystallographic perfection, the float-zone method lends itself to use as a tool for the controlled study of deliberately introduced defects and impurities in Si crystals and their effects on materials properties such as minority charge-carrier lifetime or photovoltaic conversion efficiency. Some examples of such studies are presented here. Defects we've studied include grain size, dislocations, swirl defects, and fast-cooling defects. Impurity studies have focused on H, N, Fe, and interactions between Fe and Ga. We used the bulk DC photoconductive decay lifetime characterization method and small diagnostic solar cell characterization techniques to assess material quality. The low defect and impurity concentrations obtainable by float zoning allow baseline lifetimes over 20 milliseconds and photovoltaic device efficiencies over 22%, so small effects of impurities and defects can be detected easily.

## INTRODUCTION

A variety of defects and impurities are typically present in any given sample of silicon material. So it can be difficult to conduct a controlled study of the influence of any particular defect or impurity on properties such as minority-charge-carrier lifetime $\tau$ or photovoltaic (PV) efficiency $\eta$. For example, the influence of iron may be different if boron is present because of Fe-B pair defect formation. Similarly, oxygen or carbon may influence the behavior of other impurities in Si. Therefore, it is important to conduct such studies on controlled samples where the influence of secondary effects is minimized. The float-zone (FZ) growth method can be used as a tool to obtain controlled samples.

Because there is no crucible or other heated components, very high purities and low defect levels can be achieved in baseline FZ crystals. The baseline can be controllably perturbed by the introduction of specific defects or impurities. Some of the types of defects we have studied in this way include grain size and dislocations (1), Si self-interstitial swirl defects, and fast-cooling defects (2,3). Impurity studies have focused on H (3), N (4), Fe (5), and interactions between Fe and Ga p-type dopant (6). Other defects and impurities such as vacancies, C and O, could also readily be investigated in a similar fashion.

## FZ CRYSTAL GROWTH, DOPING, AND CHARACTERIZATION PROCEDURES

All crystal growth was conducted by the high-purity, induction-heated, FZ crystal growth method. FZ growth effectively precludes large-scale introduction of other impurities such as O or C that are incorporated from crucibles or heaters when the Czochralski (CZ) method is used. It allows the effects of a particular defect or impurity to be studied in isolation from other defect/impurity effects. Ingots were zoned once in $10^{-6}$ torr vacuum or 99.999% pure argon and then (in some cases) doped p-type during the final FZ pass with 99.99999%-pure Ga.

Induction heating at 2.1 MHz was used with a single-turn, center-grounded, plate-type, water-cooled copper RF inductor to generate the floating zone. Preheating of feed rods to the temperature required for RF coupling was carried out by thermal radiation from an inductively heated cylindrical, high-density graphite block held near the bottom of the feed rod. Before all growth runs, a high vacuum ($10^{-6}$ torr) was applied to the growth chamber, even if subsequent growth was to be in argon. The graphite preheater was baked out in this vacuum environment, with the feed rod and seed removed as far as possible from the hot zone.

The low segregation coefficient of Ga ($k = 0.008$) provides very uniform p-type doping in small experimental FZ crystals, like those used in this study, when the pill doping method is used. This technique is also useful for generating controlled uniform concentrations of low-k impurities, such as Fe, Ti, or Cu in experimental crystals. In pill doping, the dopant is introduced only at the beginning of the ingot segment in which a uniform dopant distribution is desired. The required mass of dopant, m, is given by $m = (W/L_A)(C/k)V$, where W is the atomic weight of the dopant, $L_A$ is Avogadro's number, C is the desired dopant concentration in the ingot segment, k is the effective segregation coefficient, and V is the volume of the floating zone. For low k values, a very small percentage of the dopant leaves the molten zone to be incorporated into the growing ingot, and the reservoir of dopant in the melt remains essentially constant. Thus, the resulting dopant concentration is uniform along the ingot length. The method does not work well for k values near 1 (B, P), where uniform additions along the feed rod length are required for a near-constant dopant concentration in the FZ crystal.

Growth rates were typically 3 mm/min to 5 mm/min, with a crystal rotation of 10-15 rpm. All final growth passes were conducted in an argon ambient at ~0.25 Bars above atmospheric pressure and 4-5 standard liters per minute purge gas-flow rate, with the exception of studies on nitrogen effects, where nitrogen or nitrogen/argon mixed ambients were used. Some ingots were grown dislocation-free (DF) employing the usual thin-neck procedure to eliminate dislocations initiated at the seed/melt contact. Others were started from thin or thick single or multicrystalline seeds, depending on the objective.

After growth, $\tau$ was measured using the ASTM F28-75 photoconductive decay (PCD) method (7). Measurements of $\tau$ as a function of position along the ingots were done by masking off all but a 1-cm-wide window that was repositioned for each data point. For measurements of $\tau$ on wafers, the surfaces were passivated and photoconductivity changes (while immersed in HF) were detected by microwave reflection (1).

Diagnostic solar cell devices for the characterization of defect/impurity effects on cell parameters were arrays of moat-isolated mesas with diffused junctions. Junction diffusion was carried out at 850°C for 20 minutes using solid-source wafers. Photolithography was used to define Ti/Pd/Ag grids and an etched moat around each 2-mm x 2-mm. (0.04 $cm^2$), mesa-isolated cell. Aluminum back contacts were used. No texturing, surface passivation, or antireflection (AR) coatings were applied, so that the cell parameters would more closely reflect only the Si material variations. Also, by not using oxide surface passivation, we were able to maintain a relatively low maximum cell process temperature of 850°C. PV cells made in this manner from dislocation-free FZ control wafers had the following parameters measured under a Spectrolab XT10 solar simulator: open-circuit voltage $V_{oc}$ = 0.533 V, short-circuit current density $J_{sc}$ = 22.23 $mA/cm^2$, fill factor FF = ~74.3%, and $\eta$ = 8.8%. All measurements for the experimental cells were also made under the XT10 simulator and normalized to these values. After AR coating, the parameter values for a control cell (measured under standard test conditions with a Spectrolab X25 solar simulator) were as follows: $V_{oc}$ = 0.545 V, $J_{sc}$ = 31.32 $mA/cm^2$, FF = 78.4%, and $\eta$ = 13.4%. These values were not used in the normalizations, but are listed for additional information. The grid coverage for the mesa cell masks we used in this study is greater than 10%.

## EXAMPLES OF DEFECT AND IMPURITY STUDIES

### Grain-Size Effects on $\tau$ and $\eta$

Float zoning with a 2-cm-diameter and very fine-grained polycrystalline seed, cut along the diameter of a chemical-vapor deposited polycrystalline feed rod, was used to generate a set of high-purity samples with a range of grain sizes, as shown in Fig. 1. Several cooling rates were used. Wafer lifetimes (by reflected microwave PCD) were measured and correlated with grain size. The results are shown in Fig. 2. Diagnostic mesa solar cells, 2-mm-square, were also fabricated on the wafers and characterized for $\eta$, open-circuit voltage, short-circuit current, and fill factor. The cell results were also correlated with grain size (Fig. 3). Average grain size was determined from the ratio of cell area to the number of grains counted within the cell's boundaries. Electron-beam induced current (EBIC) scans were used to investigate the relative amount of carrier recombination for the different types of grain boundaries. Typical cell geometries, grain structures, and EBIC scans are shown in the photomicrographs of Fig. 4.

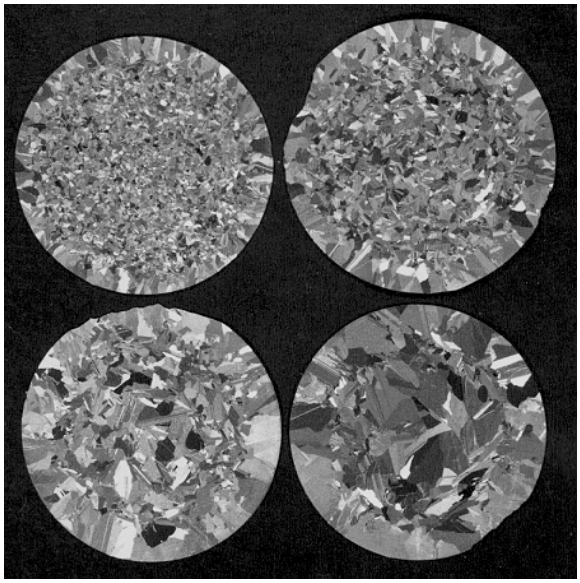

**Fig. 1.** Examples of grain sizes for a 20-mm-diameter ingot grown from a 20-mm-diameter polycrystalline seed at locations 4, 8, 16, and 32 mm from the seed attachment.

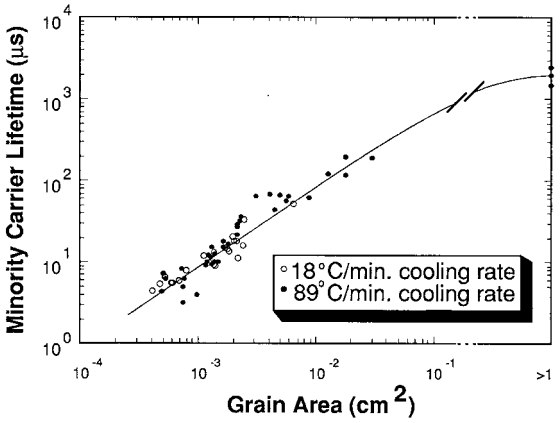


**Fig. 2.** Grain-size effect on τ for two ingot cooling rates.

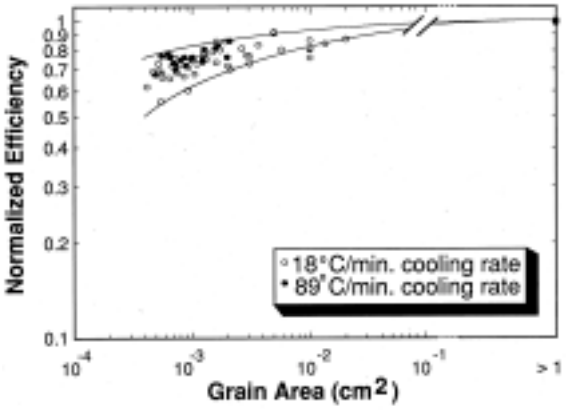


**Fig. 3.** Dependence of normalized cell efficiency on average grain area in high-purity multicrystalline silicon.

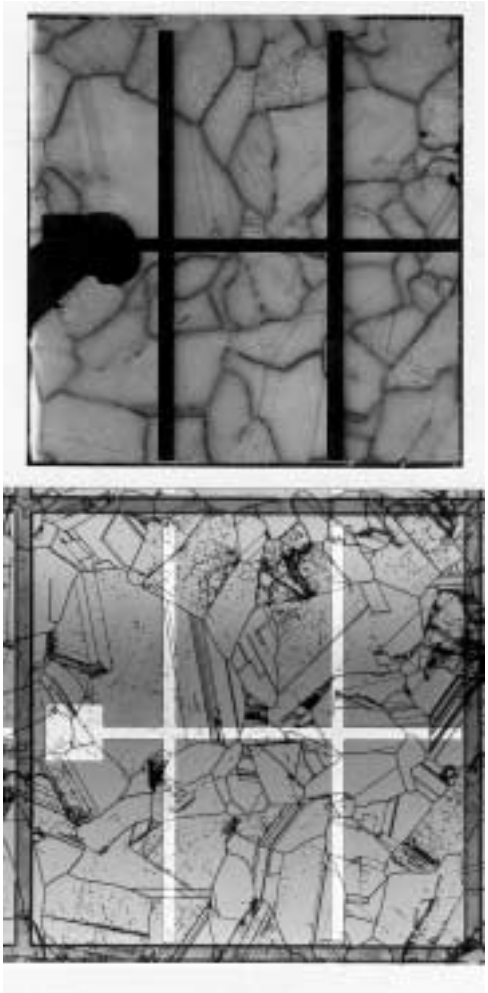

**Fig. 4.** Photomicrograph of a 2-mm x 2-mm mesa cell (bottom) and an EBIC image of the same cell (top).

We found that τ decreases with decreasing grain area, from 200 μs at 2 x $10^{-2}$ $cm^2$ grain area to 4 μs at 5 x $10^{-4}$ $cm^2$ grain area in high-purity silicon. This has important implications for thin-layer (~30 μm) Si solar cells, because it implies that if grain size is comparable to the layer thickness, τ may only be marginally adequate to allow carriers to diffuse to the contacts before recombining. The diagnostic solar cell devices showed that normalized solar cell efficiency is about 60% of the value for dislocation-free wafers at 5 x $10^{-4}$ $cm^2$ grain area (1). Again, projecting these results to thin-layer cells implies a loss of over 50% in efficiency. Light trapping will be important in thin cell structures to maximize performance.

Dislocation Effects on Cell Efficiency η

A small effect of uniform dislocation density on cell efficiency was seen (1). As shown in Fig. 5, about a 12% drop in η was observed at the largest density studied (~1.5 x $10^5$ $cm^{-2}$) as compared to the efficiency for DF control cells. The decrease was approximately linear between 3 x $10^3$ $cm^{-2}$ and 1.5 x $10^5$ $cm^{-2}$ densities. Densities higher than ~1.5 x $10^5$ $cm^{-2}$ are difficult to achieve, especially in large crystals, without low-angle grain-boundary formation and loss of single-crystal structure.

Type A and B Swirl Effects on τ

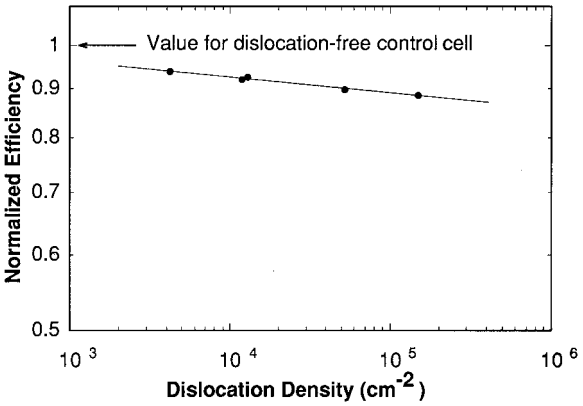


**Fig. 5.** Dependence of normalized PV cell efficiency on dislocation density in high-purity single-crystal silicon.

As the growth rate of FZ DF crystals increases, the incidence of grown-in type A and type B swirl defects (silicon self-interstitial cluster defects arranged in a helical distribution about the crystal axis) decreases. At some threshold rate, swirl defects are eliminated, leaving only type D or type I microdefects. The elimination of swirl defects has a remarkable effect on τ — more than an order of magnitude increase — from 500 μs to 10,000 μs, as the growth rate increases from 2 to 5 mm/min, as shown in Fig. 6. The decrease of swirl defects (and accompanying increase in τ) appears to be correlated with an increase in v/G, where v is the growth rate and G is the thermal gradient in the crystal near the solid/ liquid interface (about 200°C/cm for 30-mm-diameter crystals grown at 3 mm/min).

In Fig. 6, the top photographs represent longitudinal section samples removed from

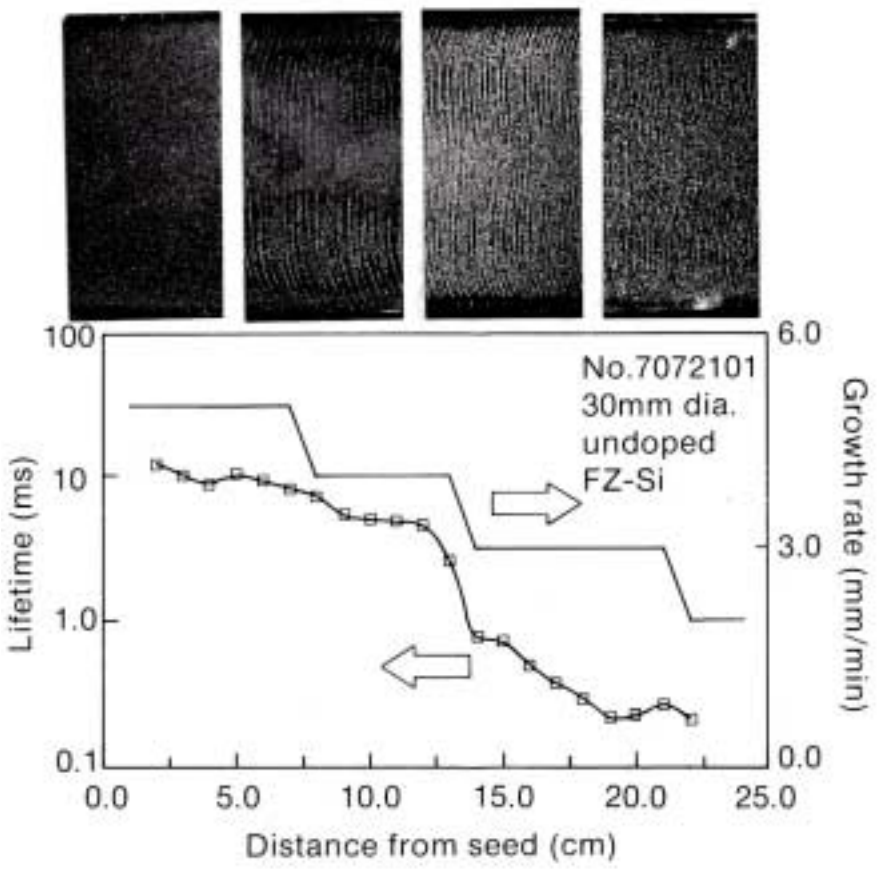


**Fig. 6**. Dependence of swirl defects and τ on growth rate of 30-mm-dia. DF crystals.

regions of the DF crystal grown at each of the four growth rates (2, 3, 4, and 5 mm/min), copper- decorated at 900°C, and defect-etched to reveal swirl defects. The height of each segment is the crystal diameter, approximately 30 mm. The increase of $\tau$ with v is independent of whether fast or slow rates are used initially. D-type microdefects are still present in the segment grown at 5 mm/min. They appear to have less of an effect on $\tau$ than A- or B-type defects, but they have not been thoroughly studied. More details about this work can be found in references (2) and (3).

Crystal Cooling Rate Effects on $\tau$

Besides growth rate, the post-solidification crystal-cooling rate also has an effect on $\tau$. The cooling rate dT/dt is the product of $v = \delta x/\delta t$ and $G = \delta T/\delta x$, or v x G, where T is temperature, t is time, and x is position along the crystal from the melt interface. When all swirl defects are eliminated by growing dislocation-free FZ crystals at an adequately large v/G, it is observed that higher values of $\tau$ are observed at slower cooling rates. The dependence is monotonic, as shown in Fig. 7, and reaches an almost constant low value when the cooling rate exceeds 600°C/min.

The data in Fig. 7 were obtained from crystals of various diameters between 6 and 52 mm, grown at 4 mm/min < v < 16 mm/min, with high enough values of v/G to eliminate swirl defects in all samples (2,3). The origin of the fast-cooling defect is not known, but it is apparently a type of quenched-in defect such as the Si vacancy or vacancy-impurity complex. To estimate the activation energy $E_a$ of the fast-cooling defect, we quenched crystals from various temperatures T, within the growth chamber, immediately after growth so that no external impurities are introduced, and measured $\tau$ on the quenched crystals. The activation energy was found from the slope of an Arrhenius plot of $1/\tau$ vs. 1000/T to be 0.31 eV (Fig. 8). This is a relatively low activation energy, and tends to imply a thermally generated point defect rather than an impurity or impurity-lattice defect cluster (since the crystals in this study were grown and heat-treated by high-purity FZ procedures instead of the furnace heat treatment procedures used in earlier studies).

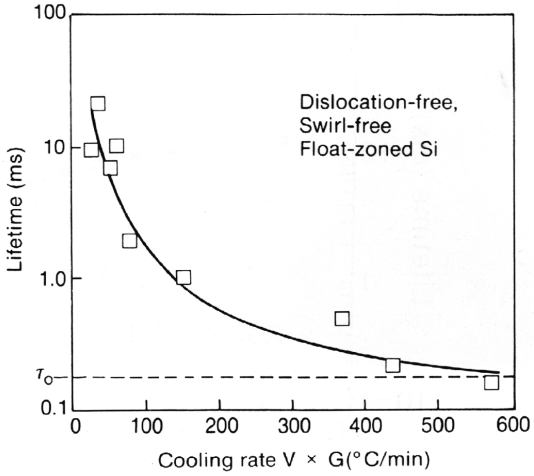


**Fig. 7.** Cooling rate effect on $\tau$ for high-purity, swirl-free FZ crystals.

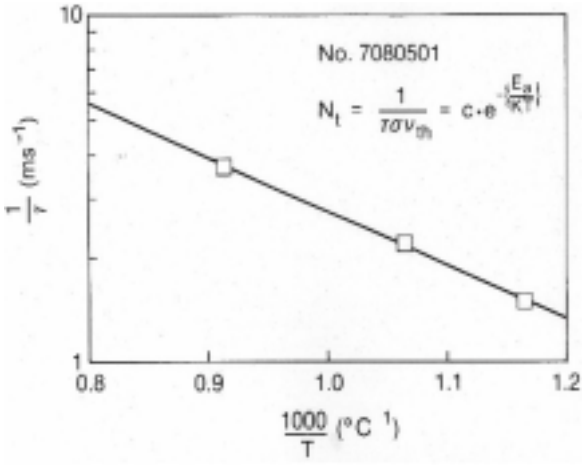


**Fig. 8.** Arrhenius plot for obtaining the activation energy of fast-cooling defects.

As crystal diameter increases, G tends to decrease as well, and higher lifetimes are favored both from swirl-defect considerations and cooling-rate considerations. A much smaller dependence of lifetime on cooling rate is observed for dislocated crystals. Additional details about our work on frozen-in defects can be found in references (2, 3), and (8).

Effects of Hydrogen Doping on $\tau$ in DF FZ Crystals

We have seen that high v/low G growth conditions effectively eliminate swirl defects and increase $\tau$. Hydrogen doping during crystal growth has also been used to eliminate swirl defects in some early studies (9). In more recent work, we grew DF FZ crystals in a 10% $H_2$/90% Ar ambient to observe the effects on lifetime and defect structure (3). X-ray {220} topographs were made of copper-decorated samples from an undoped crystal and the H-doped crystal, which were both grown at low enough v to normally result in swirl defects. The decorated swirls were clearly seen in the topograph of the undoped crystal and were absent in the topograph of the H-doped crystal. The latter, however, contained a very low density (several/$cm^2$) of large decorated defects with clear gettered regions around them (see Fig. 9), whereas the majority of the topograph exhibited a haze-like background. The measured value of $\tau$ for adjacent non-copper-decorated regions of the crystals was substantially higher for the undoped crystal (2000 μs) than for the H-doped crystal (100 μs). The explanation of the magnitude of this lifetime-reduction effect in H-doped FZ crystals is unclear, since the density of the large defects is so low. It may rather be related to the haze-like background defects that show up with Cu decoration.

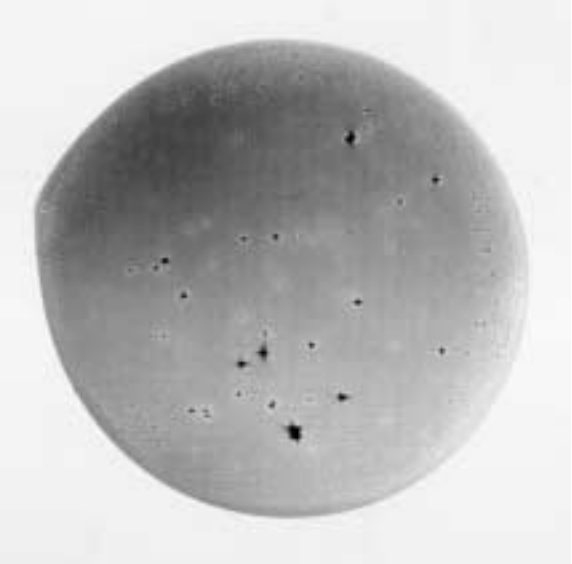

**Fig. 9.** {220} X-ray topograph of a Cu-decorated transverse wafer from a <111> FZ crystal grown in a 10% $H_2$/90% Ar ambient.

Effects of Nitrogen Doping on $\tau$

It is known that Si crystal or multicrystalline growth in $N_2$ or partial-$N_2$ atmospheres can provide mechanical strengthening (like oxygen in CZ growth) and lower purge-gas costs (nitrogen from liquid sources is about a factor of 4 less expensive than argon from liquid sources). There is not much literature on electrical effects of N in Si, especially lifetime effects. We studied some of the effects of Si growth in atmospheres containing $N_2$ on minority-charge-carrier lifetime using the FZ crystal-growth method (4). The growth ambient was changed by varying the purge gas source in increments from pure argon at the beginning of the growth process, to various compositions from the group

95% Ar/5% $N_2$, 75% Ar/25% $N_2$, 50% Ar/50% $N_2$, and 100% $N_2$. The flow rate was typically 5-6 standard liters•$min^{-1}$ with a chamber volume of 150 liters and a chamber pressure of 1.2 bar (0.2 bar above atmospheric pressure). Under these conditions, a step change in purge gas source composition results in a slowly changing ambient (about 25 minutes for a complete change, even with no mixing).

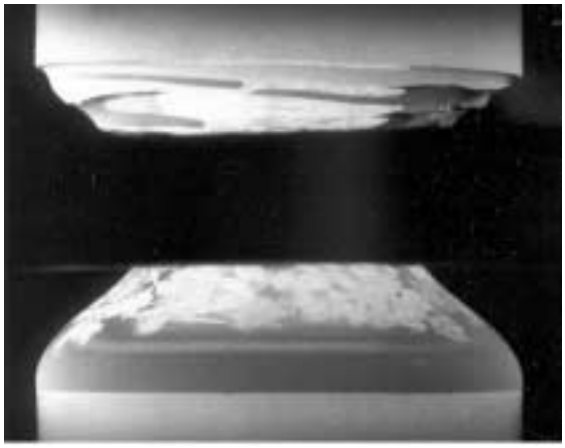

**Fig. 10.** Photograph of a 33-mm-dia. Si floating zone in a 100% N2 ambient.

We found that multicrystalline silicon ingot growth in a partial or total nitrogen ambient has a minimal degradation effect on $\tau$ (relative to multicrystalline growth in an argon ambient). Rather, $\tau$ appears to be determined predominantly by the ingot grain size, and values are near 80 μs. However, nitride compounds will form on the melt surface and on the hot feed rod and crystal surfaces, as depicted in Fig. 10. Growth can be conducted despite the nitride formation and should be easier in casting or directional solidification where the top of the melt is far from the ingot interface. The concentration of N in multicrystalline ingots grown in a 100% $N_2$ purge gas approaches $1\times10^{16}$ atoms•$cm^{-3}$. Multicrystalline growth is of interest for PV applications.

For DF, single-crystal growth, the effect of $N_2$ on $\tau$ is minimal and can even be beneficial (values around 4,000 μs were observed), provided that the amount of $N_2$ in the purge gas is kept below the level at which nitride compounds form in the melt and nucleate dislocations. A beneficial effect of $N_2$ is the elimination of swirl-type defects, and this is probably the reason high lifetimes are obtained. We have not established the upper limit of $N_2$ content in the purge gas for steady-state "start-to-finish" DF growth. At 10% $N_2$ in Ar, nitride compounds eventually form on the melt.

## Effects of Fe Doping on $\tau$ in Multicrystalline Silicon

Fe-doped multicrystalline ingots were grown by the FZ method to study Fe effects on $\tau$ and grain structure (5). Grain structures similar to those in Fig. 1 were obtained at low Fe concentrations, but evidence of Fe precipitation and constitutional supercooling were seen at target doping levels near $1 \times 10^{16}$ $cm^{-3}$. Fe was introduced by the previously mentioned pill-doping method. We made the assumption that $k \sim 2k_o$, where $k_o \sim 1 \times 10^{-5}$ for Fe in Si. For such low k values, concentrations are uniform along the ingot length. A range of Fe concentrations, which we calculate to lie between $\sim 2 \times 10^{12}$ and $\sim 1 \times 10^{16}$ atoms/$cm^3$, was produced using m values between 0.14 mg and 0.5 g. The mass of Fe dopant was held between a 20-mm-dia. multicrystalline seed, similar to the ones used in the grain boundary studies, and the bottom of the feed rod. No additional electrically active dopants were introduced.

Lifetimes were observed to decrease monotonically with increasing Fe content for similar grain sizes (from ~10 μs to 2 μs for $< 10^{-3}$ $cm^2$ grains, from ~30 μs to 2 μs for ~5 x $10^{-3}$ $cm^2$ grains, and from ~300 μs to 2 μs for $> 10^{-2}$ $cm^2$ grains) as the Fe content increased to 1 x $10^{16}$ atoms/$cm^3$. Details are shown in Fig. 11. We had previously observed that grain size has a strong effect on lifetime (1), as shown in Fig. 2.

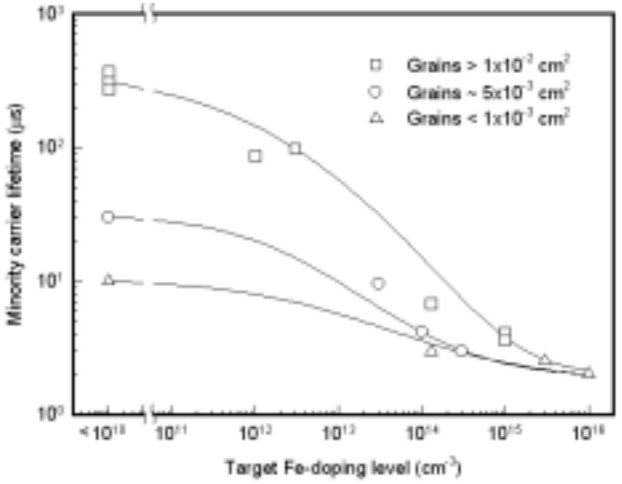


**Fig. 11.** Measured τ versus target Fe doping level for FZ multicrystalline ingots with various grain sizes.

Effects of Fe-Ga Pair Defects on τ in DF Crystals

We deliberately co-doped silicon with Fe and Ga during dislocation-free FZ crystal growth to determine the effect of Fe-Ga pair defects on τ (10). Ga is an important alternative p-type dopant to B for growth configurations that are semicontinuous in nature, such as float zoning, electromagnetic semicontinuous casting, or continuously melt replenished CZ growth. Because of its low segregation coefficient, it easily produces uniform doping in such configurations and is compatible with high-lifetime silicon growth (2). Fe is a common impurity in Si, so the study of Fe-Ga pair defects has considerable relevance. We observed a bulk minority-carrier lifetime killing effect in the Fe-Ga co-doped crystals, and were able to refine defect-energy values, and estimate defect-binding energies related to the pair defect.

A range of Fe concentrations, which we calculate to lie between ~5 x $10^{11}$ and ~1.3 x $10^{14}$ atoms/$cm^3$, was produced using pill doping m values between 0.06 mg and 17 mg. Ga concentrations between 2 x $10^{15}$ and 1 X $10^{16}$ atoms/$cm^3$ result from Ga mass values between 0.3 and 1.3 mg. Details of seeding, doping, growth, and the effects of Fe (alone) on lifetime may be found in our prior work (5).

Minority-carrier lifetime was measured on 1-cm x 1-cm x 3-cm bars cut from the as-grown crystals, which had been at room temperature for more than a month between growth and measurement. A low-injection ($<3x10^{12}$ carriers·$cm^{-3}$), YAG- or 940-nm diode-laser excited, ASTM F28-75 DC PCD method was used. Measured lifetime values of the control samples in the present study with only Ga doping (see row one in Table I) or only Fe doping (see row two in Table I) were consistent with earlier observations. The co-doped samples (rows 3–5) had lifetime values up to a factor of 20 lower than those with only Fe doping, even though very high lifetimes are obtained in Ga-doped material with no Fe, indicating a dramatic lifetime-killing effect for Fe-Ga co-doping. The measured voltage decay versus time, which is used to determine τ, was observed to be closely exponential. A Fe-Ga defect-pair phenomenon, with different properties from

Table I. Minority-Carrier Lifetime of Dislocation-Free <100> FZ Single Crystals Doped with Fe and Ga

| Crystal | Resistivity (Ω-cm) | Ga ($cm^{-3}$) | Fe Target ($cm^{-3}$) | Lifetime (μs) |
|---|---|---|---|---|
| 41121 a | 3.5 | $3.8 \times 10^{15}$ | 0 | >1400 |
| 51129-1 | 24,000 | 0 | $1.2 \times 10^{14}$ | 12 |
| 70515 | 6 | $2.2 \times 10^{15}$ | $4.8 \times 10^{11}$ | 2.2 |
| 51212-la | 4.1 | $3.3 \times 10^{15}$ | $1.3 \times 10^{14}$ | 0.40 |
| 51212-lb | 1.4 | $1 \times 10^{16}$ | $1.3 \times 10^{14}$ | 0.34 |

those of the much-studied Fe-B pair defect, appears to be responsible for the lifetime-killing effect, and a variety of additional characterization methods were used to study the phenomenon.

Deep-level transient spectroscopy (DLTS) was conducted on the $1 \times 10^{16}$ $cm^{-3}$ Ga and $1.3 \times 10^{14}$ $cm^{-3}$ Fe co-doped sample to examine the energy-band defect levels of the pairing defect. The sample was cooled under -5 V reverse bias (ensuring detection of both metastable configurations of the Fe-Ga pair), and DLTS was performed. The results (see Fig. 12) indicate defect energies (relative to the valance band) equal to 0.10 and 0.21 eV, defect concentrations of $9.8 \times 10^{12}$ and $7.4 \times 10^{13}$ $cm^{-3}$, and hole-capture

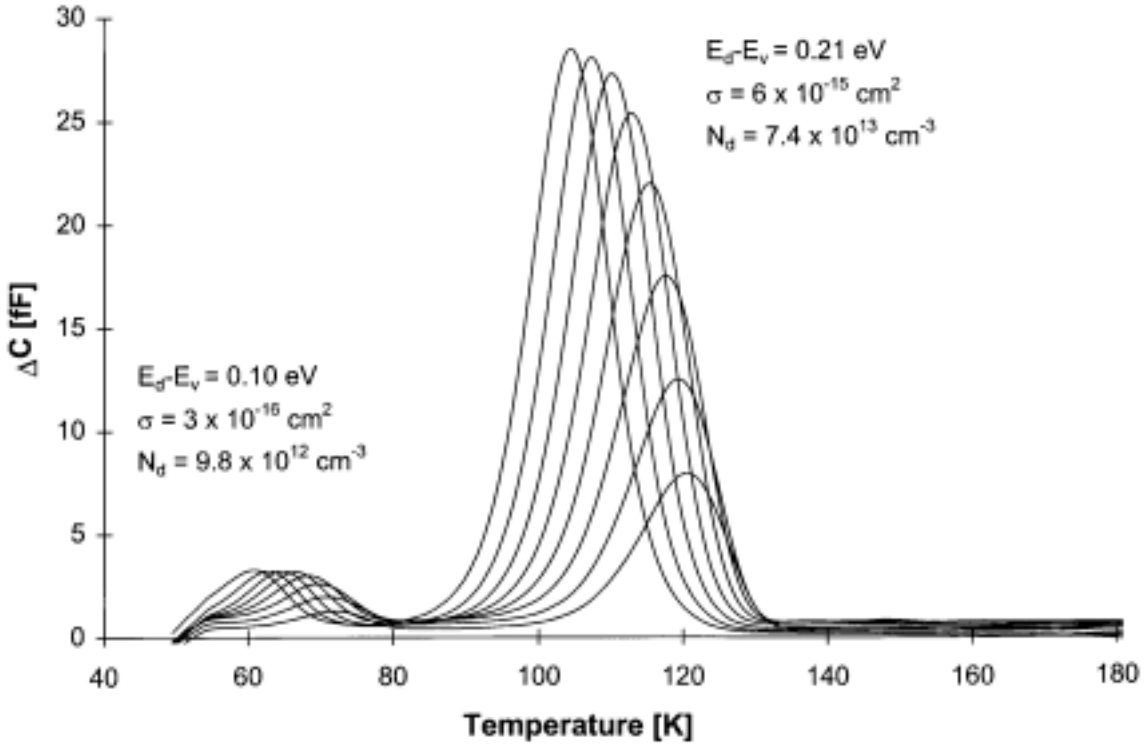


**Fig. 12.** High-energy-resolution DLTS spectra for a dislocation-free FZ silicon sample co-doped with $1 \times 10^{16}$ $cm^{-3}$ Ga and $1.3 \times 10^{14}$ $cm^{-3}$ Fe.

cross-sections (at $T = \infty$) equal to $3 \times 10^{-16}$ and $6 \times 10^{-15}$ $cm^2$, respectively.

To confirm that the lower lifetimes in co-doped samples are indeed due to Fe-Ga pair defects, we performed low-temperature (50°–250°C) annealing experiments. The results of heating to several different prescribed temperatures and then quickly quenching to room temperature (for $\tau$ measurement) are shown as an Arrhenius plot of $1/\tau$ vs. $1/T$ in Fig. 13. Dissociation of Fe-Ga pairs at higher temperature leads to higher lifetime, confirming that interstitial Fe has less recombination activity than the Fe-Ga pair defects.

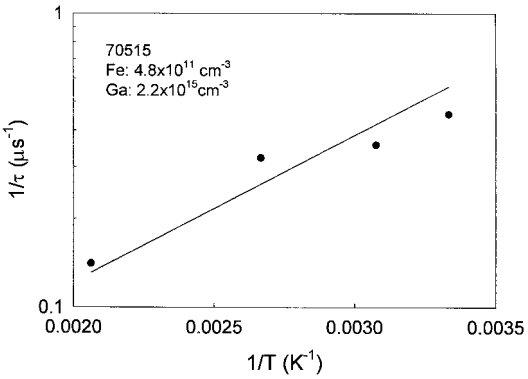


**Fig. 13.** Lifetime versus annealing temperature for a dislocation-free FZ Si crystal co-doped with Fe: $4.8 \times 10^{11}$ $cm^{-3}$, Ga: $2.2 \times 10^{15}$ $cm^{-3}$.

Because Fe-Ga defects exhibit configurational bistability, we could not derive the binding energies $E^b$ of Fe-Ga from the annealing experiment alone. But with information from the DLTS measurements, we were able to deduce binding energies of 0.09 eV and 0.15 eV for the defects at energy levels $E_v + 0.1$ eV and $E_v + 0.21$ eV, respectively. These binding energies are surprisingly low, but consistent with the ease of formation.

## SUMMARY AND DISCUSSION

A few examples of the types of defect and impurity studies that can be done with controlled silicon samples generated by the FZ method have been presented. Examples of defects included grain boundaries, dislocations, swirl defects, and fast-cooling defects. Examples of impurities included H, N, Fe, and Fe-Ga combinations. Other types of controlled samples could be generated this way. The diagram in Fig. 14 qualitatively summarizes the effects of defects, impurities, and the main growth parameters on minority-carrier lifetime in high-purity silicon.

Using the knowledge gained about defect and impurity effects on $\tau$, coupled with their relationship to crystal growth parameters, we have been able to obtain FZ Si crystals with very high $\tau$ (Fig. 15). Undoped crystal lifetimes of over 20 msec were seen. Auger recombination limits $\tau$ at high doping levels, but it is somewhat puzzling why Shockley Read Hall recombination limits the lifetime to the extent it does at the lighter doping levels. Lifetime is an important parameter in several device applications, including photovoltaics, and controlled sample generation by the FZ technique has proven to be a valuable tool for studying impurity, defect, and growth parameter effects on lifetime.

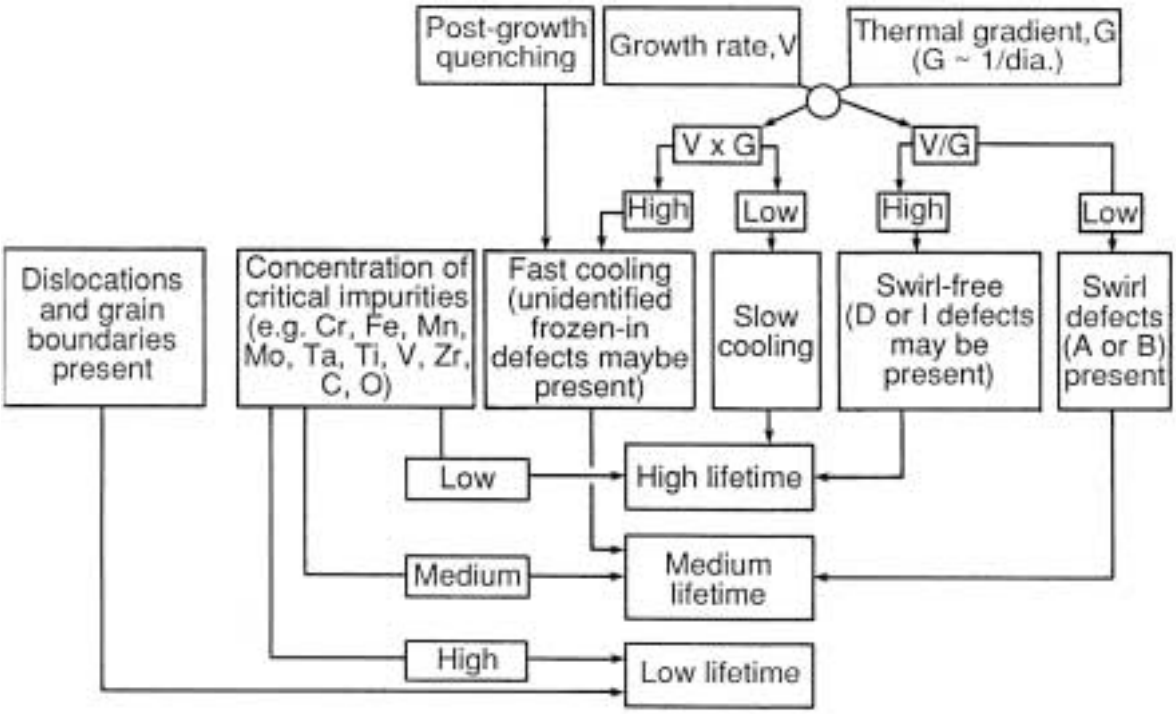


**Fig. 14.** A summary of defect, impurity, and growth parameter effects on Si lifetime.

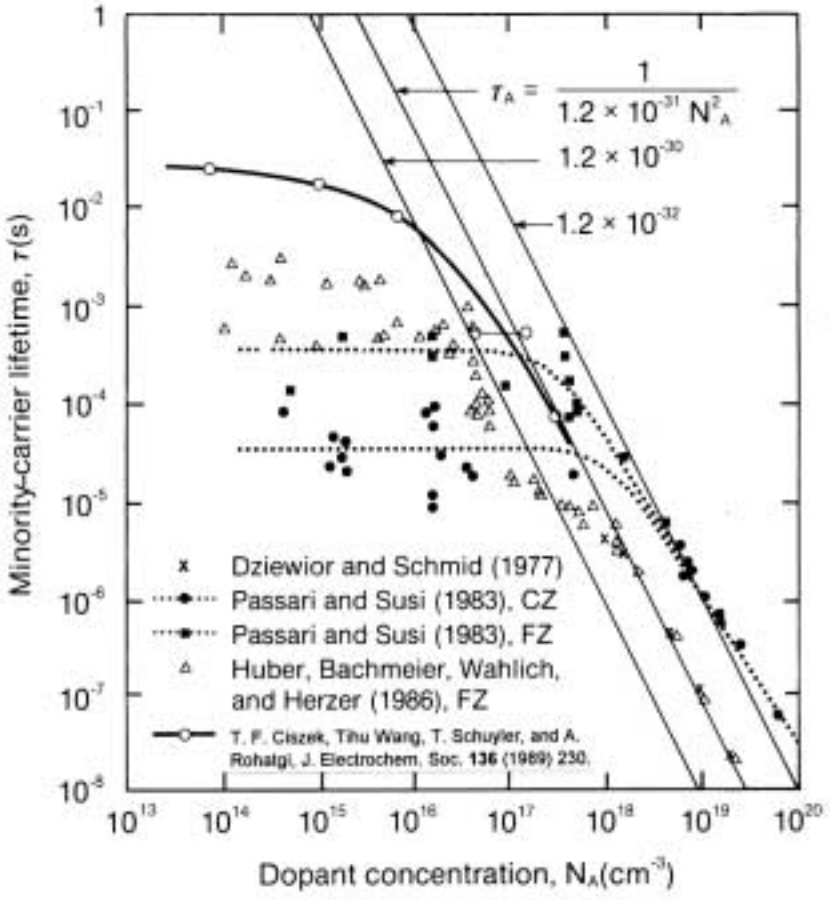


**Fig. 15**. The dependence of τ on doping level.

ACKNOWLEDGMENTS

This project was supported by the U.S. Department of Energy under Contract No. DE-AC36-98-GO10337 to NREL. The authors thank the many co-workers who have contributed to this activity, especially T. Schuyler, T. Bekkedahl, A. Rohatgi, R.W. Burrows, C. Akers, R. Matson, and W.A. Doolittle.

REFERENCES

1. T.F. Ciszek, T.H. Wang, R.W. Burrows, X. Wu, J. Alleman, Y.S. Tsuo, and T. Bekkedahl, "Grain Boundary and Dislocation Effects on the PV Performance of High-Purity Silicon," in: *23th IEEE Photovoltaic Specialists Conf. Record, Louisville, 1993* (IEEE, New York, 1993) pp. 101-105.
2. T.F. Ciszek, Tihu Wang, T. Schuyler, and A. Rohatgi, "Some Effects of Crystal Growth Parameters on Minority Carrier Lifetime in Float-Zoned Silicon," *J. Electrochem. Soc*. **136** (1989) pp. 230-234.
3. T.H. Wang, T.F. Ciszek, and T. Schuyler, "Charge Carrier Recombination Centers in High-Purity, Dislocation-Free, Float-Zoned Silicon Due to Growth-Induced Microdefects," *J. of Crystal Growth* **109** (1991) pp. 155-161.
4. T.F. Ciszek, T.H. Wang, R.W. Burrows, T. Bekkedahl, M.I. Symko, and J.D. Webb, "Effect of nitrogen doping on microdefects and minority charge carrier lifetime of high-purity, dislocation-free and multicrystalline silicon," *Solar Energy Mat. and Solar Cells* **41/42**, (1996) pp. 61-70.
5. T.F. Ciszek, T.H. Wang, R.K. Ahrenkiel, and R. Matson, "Properties of Iron-Doped Multicrystalline Silicon Grown by the Float-Zone Technique," in: *25th IEEE Photovoltaic Specialist Conf. Record, Washington D.C. May 13-17, 1996* (IEEE, New Jersey, 1996) pp. 737-739.
6. T.F. Ciszek, T.H. Wang, W.A. Doolittle, and A. Rohatgi, "Iron-Gallium Pair Defects in Float-Zoned Silicon," in: High Purity Silicon V, Eds. C.L. Claeys, P. Rai-Choudhury, M. Watanabe, P. Stallhofer, and H.J. Dawson (The Electrochemical Soc., Proceedings Volume 98-13, New Jersey, 1998) pp. 230-240.
7. ASTM F28-91 Standard, *1993 Annual Book of ASTM Standards*, Vol. 10.05, p. 30, American Society for Testing and Materials, Philadelphia (1993).
8. T.H. Wang, T.F. Ciszek, and R.K. Ahrenkiel, "Characterization of High-Purity Silicon with the Photoconductivity Decay and Photoluminescence Analysis Techniques," in: High Purity Silicon IV, Eds. C.L. Claeys, P. Rai-Choudhury, P. Stallhofer, J.E. Maurtis (The Electrochemical Soc. Proceedings Volume 96-13, New Jersey, 1996) pp. 462-469.
9. T.F. Ciszek, "Copper Decoration and X-ray Topography of Point Defects in Dislocation-Free Silicon Crystals Grown Under Various Conditions," in: Semiconductor Silicon 1973, Eds. H.R. Huff and R.R. Burgess (The Electrochemical Soc., Chicago 1973) pp. 150-160.
10. T.F. Ciszek, T.H. Wang, W.A. Doolittle, and A. Rohatgi, "Iron-Gallium Pair Defects in Float-Zoned Silicon," in: High Purity Silicon V, Eds. C.L. Claeys, P. Rai-Choudhury, M. Watanabe, P. Stallhofer, and H.J. Dawson (The Electrochemical Soc., Proceedings Volume 98-13, New Jersey, 1998) pp. 230-240.

# REPORT DOCUMENTATION PAGE

*Form Approved*
*OMB NO. 0704-0188*



| 1. AGENCY USE ONLY (Leave blank) | 2. REPORT DATE | 3. REPORT TYPE AND DATES COVERED |
|---|---|---|
| | June 2000 | conference paper |

4. TITLE AND SUBTITLE
Silicon Float-Zone Crystal Growth as a Tool for the Study of Defects and Impurities

5. FUNDING NUMBERS
C
TA: PV004801

6. AUTHOR(S)
T.F. Ciszek and T.H. Wang

7. PERFORMING ORGANIZATION NAME(S) AND ADDRESS(ES)

8. PERFORMING ORGANIZATION REPORT NUMBER

9. SPONSORING/MONITORING AGENCY NAME(S) AND ADDRESS(ES)
National Renewable Energy Laboratory
1617 Cole Blvd.
Golden, CO 80401-3393

10. SPONSORING/MONITORING AGENCY REPORT NUMBER
CP-520-28569

11. SUPPLEMENTARY NOTES

12a. DISTRIBUTION/AVAILABILITY STATEMENT
National Technical Information Service
U.S. Department of Commerce
5285 Port Royal Road
Springfield, VA 22161

12b. DISTRIBUTION CODE

13. ABSTRACT *(Maximum 200 words)*
Because of its ability to produce silicon crystals of exceptionally high purity and crystallographic perfection, the float-zone method lends itself to use as a tool for the controlled study of deliberately introduced defects and impurities in Si crystals and their effects on materials properties such as minority charge-carrier lifetime or photovoltaic conversion efficiency. Some examples of such studies are presented here. Defects we've studied include grain size, dislocations, swirl defects, and fast-cooling defects. Impurity studies have focused on H, N, Fe, and interactions between Fe and Ga. We used the bulk DC photoconductive decay lifetime characterization method and small diagnostic solar cell characterization techniques to assess material quality. The low defect and impurity concentrations obtainable by float zoning allow baseline lifetimes over 20 milliseconds and photovoltaic device efficiencies over 22%; therefore, small effects of impurities and defects can be detected easily.

14. SUBJECT TERMS
photovoltaics ; float-zone crystal growth ; defects and impurities ; minority charge-carrier lifetime ; photovoltaic conversion efficiency ; photoconductive decay ; characterization

15. NUMBER OF PAGES

16. PRICE CODE

| 17. SECURITY CLASSIFICATION OF REPORT | 18. SECURITY CLASSIFICATION OF THIS PAGE | 19. SECURITY CLASSIFICATION OF ABSTRACT | 20. LIMITATION OF ABSTRACT |
|---|---|---|---|
| Unclassified | Unclassified | Unclassified | UL |